BJ Cell

Biochem. J. (2013) **450**, 365–373 (Printed in Great Britain) doi:10.1042/BJ20121022

online data

Extracellular calcium influx activates adenylate cyclase 1 and potentiates insulin secretion in MIN6 cells

Tetsuya KITAGUCHI*†‡[1], Manami OYA§, Yoshiko WADA*†, Takashi TSUBOI§ and Atsushi MIYAWAKI*†[1]

*Life Function and Dynamics, ERATO, JST (Japan Science and Technology Agency), 2-1 Hirosawa, Wako, Saitama 351-0198, Japan, †Laboratory for Cell Function and Dynamics, Advanced Technology Development Group, Brain Science Institute, RIKEN, 2-1 Hirosawa, Wako, Saitama 351-0198, Japan, ‡Cell Signaling Group, Waseda Bioscience Research Institute in Singapore (WABOIS), Waseda University, 11 Biopolis Way, #05-01/02 Helios, Singapore 138667, Singapore, and §Department of Life Sciences, Graduate School of Arts and Sciences, The University of Tokyo, 3-8-1 Komaba, Meguro, Tokyo 153-8902, Japan

Intracellular cAMP and Ca^{2+} are important second messengers that regulate insulin secretion in pancreatic β-cells; however, the molecular mechanism underlying their mutual interaction for exocytosis is not fully understood. In the present study, we investigated the interplay between intracellular cAMP and Ca^{2+} concentrations ($[cAMP]_i$ and $[Ca^{2+}]_i$ respectively) in the pancreatic β-cell line MIN6 using total internal reflection fluorescence microscopy. For measuring $[cAMP]_i$, we developed a genetically encoded yellow fluorescent biosensor for cAMP [Flamindo (fluorescent cAMP indicator)], which changes fluorescence intensity with cAMP binding. Application of high-KCl or glucose to MIN6 cells induced the elevation of $[cAMP]_i$ and exocytosis. Furthermore, application of an L-type Ca^{2+} channel agonist or ionomycin to induce extracellular Ca^{2+} influx evoked the elevation of $[cAMP]_i$, whereas application of carbachol or thapsigargin, which mobilize Ca^{2+} from internal stores, did not evoke the elevation of $[cAMP]_i$. We performed RT (reverse transcription)–PCR analysis and found that Ca^{2+}-sensitive *Adcy1* (adenylate cyclase 1) was expressed in MIN6 cells. Knockdown of endogenous ADCY1 by small interference RNA significantly suppressed glucose-induced exocytosis and the elevation of both $[cAMP]_i$ and $[Ca^{2+}]_i$. Taken together, the findings of the present study demonstrate that ADCY1 plays an important role in the control of pancreatic β-cell cAMP homoeostasis and insulin secretion.

Key words: calcium, cAMP, exchange protein directly activated by cAMP 1 (Epac1), exocytosis, fluorescence microscopy, insulin, total internal reflection, yellow fluorescent protein.

INTRODUCTION

In pancreatic β-cells, glucose-stimulated insulin secretion consists of a transient phase followed by a sustained phase. These two phases correspond to 'triggering' and 'amplifying' pathways respectively [1,2]. In the triggering pathway, the increase in cytosolic ATP concentration via glucose metabolism in mitochondria leads to plasma membrane depolarization by closure of the K_{ATP} channel (ATP-sensitive K^+ channel). Depolarization induces the opening of L-type VOCCs (voltage-operated Ca^{2+} channels), which results in Ca^{2+} entry and subsequent insulin secretion by fusion of secretory vesicles to the plasma membrane. Meanwhile, glucose activates the metabolic amplifying pathway that is independent of K_{ATP} channels or further rises in intracellular Ca^{2+} concentrations ($[Ca^{2+}]_i$), but which does augment the insulin secretory response to the triggering Ca^{2+} signal [3].

Ca^{2+} and cAMP are ubiquitous second messengers that mediate many cellular functions, including exocytosis, cell migration, cardiac contractility, platelet aggregation and memory formation [4]. An elevation of intracellular cAMP concentration ($[cAMP]_i$) causes various Ca^{2+}-related events, including Ca^{2+} influx through VOCCs, Ca^{2+} mobilization from internal Ca^{2+} stores and activation of Ca^{2+}-activated non-selective cation channels for facilitating exocytotic events [5]. In contrast, Ca^{2+}-elevating stimulation, such as high KCl or glucose, increases not only $[Ca^{2+}]_i$ but also $[cAMP]_i$ in insulin-secreting cells [6]. Therefore it is intriguing to study how the mutual interaction between $[cAMP]_i$ and $[Ca^{2+}]_i$ is regulated during insulin secretion.

Fluorescently labelled dense-core vesicle cargoes or exo/endocytotic proteins were observed in combination with Ca^{2+} near the plasma membrane by using dual-colour TIRF (total internal reflection fluorescence) microscopy [7–9]. Because TIRF microscopy allows us to acquire fluorescence images with a high axial resolution (approximately 100 nm) at the cell–substratum interface, cellular events in the vicinity of the plasma membrane are clearly visualized. Thus, to clarify the interplay between cAMP and Ca^{2+} exocytosis in the pancreatic β-cell line MIN6, we used TIRF microscopy. Although several genetically encoded indicators for cAMP have been developed using CFP (cyan fluorescent protein) and YFP (yellow fluorescent protein) as a FRET (Förster resonance energy transfer) donor and acceptor [10–13], it is not easy to obtain their signals with high signal-to-noise ratio in TIRF microscopy. In the present study, we developed a new yellow florescent indicator for cAMP [Flamindo (fluorescent cAMP indicator)]. Flamindo changes its fluorescence intensity according to the concentration of cAMP. Flamindo uses the conformational change of the inserted cAMP-binding domain derived from mouse Epac1 (exchange protein directly activated by cAMP 1) induced by cAMP binding in the vicinity of the chromophore of a YFP variant Citrine. The elevation of $[cAMP]_i$ induced a decrease in fluorescence intensity from Flamindo-expressing COS7 cells. Using MIN6 cells that expressed

Abbreviations used: ADCY, adenylate cyclase; 8-Br-cAMP, 8-bromo-cAMP; CCD, charge-coupled device; Cch, carbachol; DDA, 2′,5′-dideoxyadenosine; DMEM, Dulbecco's modified Eagle's medium; EMCCD, electron multiplier-CCD; Epac1, exchange protein directly activated by cAMP 1; FBS, fetal bovine serum; Flamindo, fluorescent cAMP indicator; FRET, Förster resonance energy transfer; GAP43, growth-associated protein 43; GFP, green fluorescent protein; hNPY, human neuropeptide Y; IBMX, isobutylmethylxanthine; K_{ATP} channel, ATP-sensitive K^+ channel; NPY, neuropeptide Y; PM-Flamindo, plasma-membrane-targeted Flamindo; RB, Ringer's buffer; RT, reverse transcription; siRNA, small interfering RNA; TG, thapsigargin; TIRF, total internal reflection fluorescence; VOCC, voltage-operated Ca^{2+} channel; YFP, yellow fluorescent protein.

[1] Correspondence may be addressed to either of these authors (email kitaguct@aoni.waseda.jp or matsushi@brain.riken.jp).

Flamindo, we observed that glucose stimulation activated Ca^{2+}-sensitive ADCY (adenylate cyclase) 1 and induced the elevation of $[cAMP]_i$. We also show that the ADCY1 response is dependent on an $[Ca^{2+}]_i$ increase due to a Ca^{2+} influx. Because ADCY1 is located on the plasma membrane, the enzyme is supposed to relay the Ca^{2+} influx to cAMP generation for efficient secretion of insulin. The findings of the present study suggest that ADCY1 is essential for the amplifying pathway during glucose-stimulated insulin secretion in the MIN6 pancreatic β-cell line.

EXPERIMENTAL

Chemicals

cAMP, cGMP, forskolin, 8-Br-cAMP (8-bromo-cAMP), IBMX (isobutylmethylxanthine), BAY K 8644, ionomycin, Cch (carbachol) and TG (thapsigargin) were purchased from Calbiochem. DDA (2′,5′-dideoxyadenosine) was purchased from Sigma–Aldrich.

Plasmid constructions

The cDNA for a variant of YFP, Citrine, was engineered to contain SacII and EcoRI restriction enzyme sites at the position of Tyr^{145} using three separate PCRs [14]. The 5′ portion of the Citrine DNA was amplified by the first PCR using a sense primer containing an HindIII site and a reverse primer containing both SacII and EcoRI sites. The second PCR was performed to amplify the 3′ portion of the Citrine DNA with a sense primer containing both SacII and EcoRI sites and a reverse primer containing an XhoI site. These two PCR products were combined and amplified with the HindIII-containing sense primer and the XhoI-containing reverse primers. The resultant PCR product encoding the modified Citrine was cloned into the HindIII/XhoI sites in the pcDNA3 vector (Invitrogen). The gene for the cAMP-binding domain of mouse Epac1 (amino acids 157–316) was amplified with an SacII-containing sense primer and an EcoRI-containing reverse primer [15]. The resultant product was cloned into the SacII/EcoRI sites of Citrine to yield the construct of Flamindo for mammalian expression. For plasma-membrane-targeted expression, the annealed primers encoding 20 amino acids of the GAP43 (growth-associated protein 43; neuromodulin) fragment was cloned into the 5′-terminal HindIII site of Flamindo. Flamindo was amplified with BamHI and XhoI sites containing primers and the resultant product was cloned in-frame into BamHI/XhoI sites of the $pRSET_B$ vector (Invitrogen) for bacterial expression.

To visualize exocytosis, cDNA of hNPY [human NPY (neuropeptide Y); 1–97 amino acids] fused to far-red fluorescent protein, mKate (TagFP635, Evrogen), was generated [16]. To create NPY–mKate, hNPY was amplified with primers containing HindIII and KpnI sites, and the far-red fluorescent protein mKate with primers containing BamHI and EcoRI sites. Both fragments were cloned into HindIII/KpnI sites and BamHI/EcoRI sites in pcDNA3.1(+) (Invitrogen) sequentially.

Mouse *Adcy1* was amplified from a mouse brain cDNA by PCR. The cDNA fragment of *Adcy1* was finally inserted into the pEF-BOS vector [17] with a FLAG-tag at the C-terminus. The sequence of all plasmid inserts was verified by automated sequencing.

Protein expression and *in vitro* spectroscopy

Flamindo in the $pRSET_B$ vector was transformed into *Escherichia coli* JM109 (DE3) cells, and Flamindo protein fused to the N-terminal polyhistidine tag was expressed. After 4 days of culture in LB (Luria–Bertani) medium supplemented with 100 μg/ml ampicillin at 20 °C, cells were harvested by centrifugation (5000 ***g*** for 5 min at 4 °C). The harvested bacterial pellet was lysed by three freeze–thaw cycles and sonication in PBS supplemented with 40 μg/ml lysozyme. After centrifugation of bacterial lysates (5000 ***g*** for 30 min at 4 °C), Flamindo protein was purified from the supernatants using an Ni-NTA (Ni^{2+}-nitrilotriacetate) agarose column (Qiagen) followed by a PD-10 gel-filtration column (GE Healthcare) for removal of imidazole against Hepes buffer [150 mM KCl and 50 mM Hepes-KOH (pH 7.4)]. For pH titration experiments, purified Flamindo in Hepes buffer was diluted 100-fold or more in buffer containing 100 mM acetate (pH 4), citrate (pH 5), NaH_2PO_4 (pH 6), Hepes (pH 7 and 8) or glycine (pH 9 and 10). All measurements of absorption of purified Flamindo protein were performed using an U-3310 spectrophotometer (Hitachi), and fluorescence measurements were made using an F-4500 fluorescence spectrophotometer (Hitachi).

Cell culture and transfection

COS7 and MIN6 cells [18] were plated on to poly-L-lysine-coated glass coverslips in 35-mm dishes or 100-mm dishes and grown to 50–90 % confluency. COS7 cells were cultured in DMEM (Dulbeco's modified Eagle's medium) containing 10 % (v/v) heat-inactivated FBS (fetal bovine serum) and MIN6 cells were cultured in DMEM containing 15 % (v/v) FBS supplemented with 50 μM 2-mercaptoethanol. For imaging of cAMP and/or exocytosis, cells in glass coverslips in 35-mm dishes were transfected with 2 μg of Flamindo and/or 2 μg of NPY–mKate expression vectors by using Lipofectamine™ 2000 (Invitrogen). For Ca^{2+} imaging, the cells in glass coverslips in 35-mm dishes were loaded with 5 μM Fluo3/AM (acetoxymethyl ester) (Sigma–Aldrich) for 40 min at 37 °C. The cells were then washed twice before imaging.

To knockdown ADCY1, we transfected with 60 pmol (for the 35-mm dish) or 400 pmol (for the 100-mm dish) of MISSION siRNA (small interfering RNA) (Sigma–Aldrich) against mouse ADCY1 or a matched siRNA negative control (scramble RNA) with or without 15 μg (for the 100-mm dish) ADCY1–FLAG expression vector for 16 h. The sequences of siRNAs chemically synthesized are listed in Supplementary Table S1 (at http://www.biochemj.org/bj/450/bj4500365add.htm). The cells were used for experiments 48 h after transfection.

Imaging of COS7 cells was performed in Phenol-Red-free DMEM at room temperature (22 °C). Imaging of MIN6 cells was performed in modified RB (Ringer's buffer) containing 3 mM glucose [RB: 130 mM NaCl, 3 mM KCl, 5 mM $CaCl_2$, 1.5 mM $MgCl_2$ and 10 mM Hepes (pH 7.4)] at 37 °C. High-KCl stimulation was achieved by perfusion with 50 mM KCl-containing RB (the NaCl concentration was reduced to maintain the osmolarity). For glucose stimulation, MIN6 cells were cultured in DMEM containing 3 mM glucose for 16 h before imaging. Imaging was performed in RB containing 3 mM glucose, and stimulated by RB containing 25 mM glucose.

Epifluorescence imaging

Between 2 and 4 days after transfection, COS7 or MIN6 cells were imaged using the Olympus IX-70 inverted microscope with a cooled CCD (charge-coupled device) camera (Cool SNAP fx, Roper Scientific) using a UApo/340 40 ×1.35 numerical aperture and an oil-immersion objective lens (Olympus). Image acquisition and analysis were performed using MetaFluor software

(Universal Imaging). A 490DF20 excitation filter, 505DRLP dichroic mirror and 535DF35 emission filter were used in single-wavelength imaging for Flamindo. Images were acquired every 5 s.

TIRF imaging

To observe the exocytosis of NPY–mKate at the single-vesicle level, we used a dual-colour TIRF microscope as described previously [19]. To excite Flamindo/Fluo3 and NPY–mKate, we used a diode-pumped solid state 488-nm (HPU50100, 20 mW, Furukawa Electronic) and 561-nm laser (85YCA020, 20 mW, Melles Griot) respectively. For simultaneous imaging of yellow/green and red fluorescence, an image splitter (Dual View; Optical Insights) divided the red and yellow/green components of the images with a 565-nm dichroic mirror (Chroma) and passed the red component through a 580-nm long pass filter (Chroma) and the yellow/green component through a 500–540-nm bandpass filter (Chroma). The images were then projected side-by-side on to an EMCCD (electron multiplier-CCD) camera (C9100-02, Hamamatsu Photonics). The laser beams were passed through an electromagnetically driven shutter (VMM-D3J, Unibritz), and the shutter was opened synchronously with the EMCCD camera exposure controlled by MetaMorph software (Molecular Devices). Images were acquired every 300 ms.

RT (reverse transcription)–PCR analysis

Total RNA was isolated from adult mouse tissues or cell cultures using the RNAeasy mini kit (Qiagen). After DNase I treatment, RT was performed with PrimeScript Reverse Transcriptase (Takara). Histone H2afz expression was measured to monitor RNA recovery [20]. The PCR was stopped and the amplified products were analysed when the products reached the log-linear phase of the amplification curve. The primers used for PCR amplification are listed in Supplementary Table S2 (at http://www.biochemj.org/bj/450/bj4500365add.htm).

Immunoblotting

Protein lysates from COS7 cells were prepared in SDS sample buffer containing 2.5 % (v/v) 2-mercaptoethanol. Proteins were electrophoresed on SDS/PAGE (10 % gels), and transferred on to Immobilon-P membranes (Millipore). Membranes were blocked with 5 % (w/v) non-fat dried skimmed milk in PBS with 0.1 % Tween 20. Antibodies against the FLAG-tag (M2) and against β-actin (AC-15) were obtained from Sigma–Aldrich. Membranes were washed six times with PBS-Tween 20, and incubated with horseradish-peroxidase-conjugated secondary antibodies (GE Healthcare). Blots were detected using an ECL (enhanced chemiluminescence) detection kit (GE Healthcare).

RESULTS

Generation of the cAMP indicator Flamindo

The single fluorescent protein-based Ca^{2+} indicator Camgaroo uses a Ca^{2+}-dependent conformational change of calmodulin inserted into Citrine at Tyr^{145} [21,22]. Previous studies have shown that the binding of cAMP to mouse Epac1 induced a conformational change in the protein [23]. For the development of single fluorescent protein-based cAMP indicators, we inserted the cAMP-binding domain of mouse Epac1 at Tyr^{145} in Citrine (Supplementary Figure S1 at http://www.biochemj.org/bj/450/bj4500365add.htm) [21]. We used different lengths of the insert as well as different linkers. Among 12 chimaeric proteins tested, one displayed the largest change in florescence intensity upon addition of cAMP. The protein was named Flamindo (Figure 1).

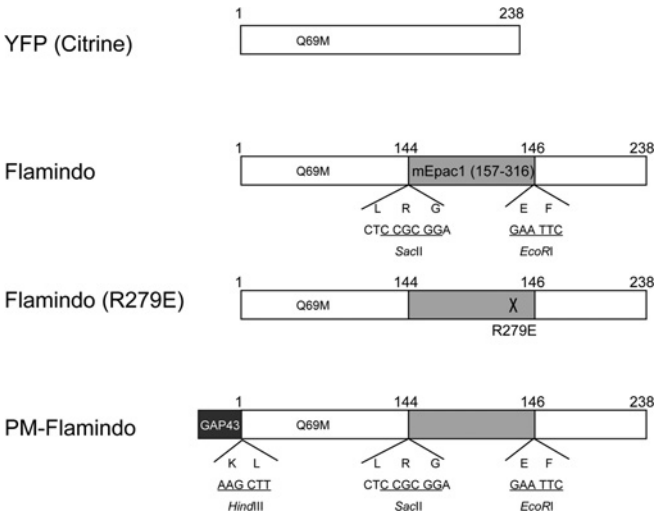

Figure 1 Schematic drawing of the structure of Flamindo

Amino acid sequences of linkers derived from restriction enzyme sites are shown underneath the structures. Flamindo was created by Citrine inserted into the cAMP-binding domain of mouse Epac1 (mEpac1), a cAMP-dependent guanidine-exchange factor. Flamindo (R279E) contains a mutation that abolishes cAMP binding. GAP43 (neuromodulin) was fused to the N-terminal of Flamindo for measuring the cAMP concentration at the plasma membrane.

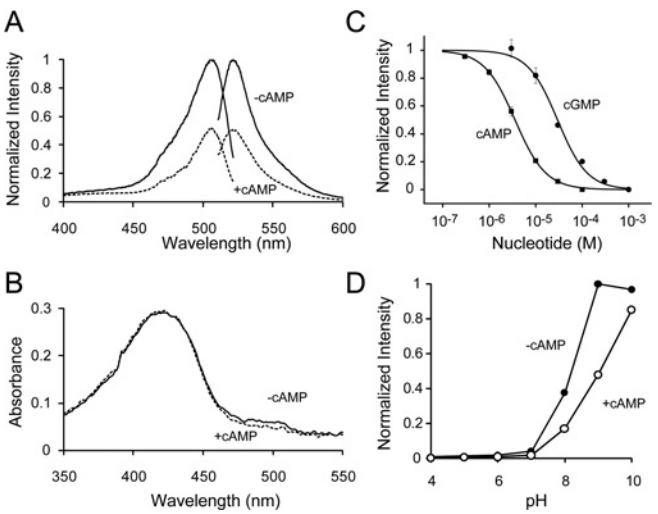

Figure 2 Characteristics of Flamindo

(**A**) Fluorescence excitation and emission spectra of Flamindo with (broken lines) or without (solid lines) 1 mM cAMP. (**B**) Absorbance spectrum of Flamindo with (broken line) or without (solid line) 1 mM cAMP. (**C**) Dose–response curve of Flamindo for cAMP (■) and cGMP (●). (**D**) pH-dependent fluorescence intensity changes of Flamindo with (○) or without (●) 1 mM cAMP. All spectra and data points were normalized to a maximum value of 1.0. Results shown are the means ± S.E.M.

Spectral properties of Flamindo

We measured the fluorescence excitation and emission spectra of purified bacterially expressed recombinant Flamindo protein (Figure 2A). When excited at 506 nm, Flamindo showed an emission maximum at 521 nm. Addition of maximal doses of

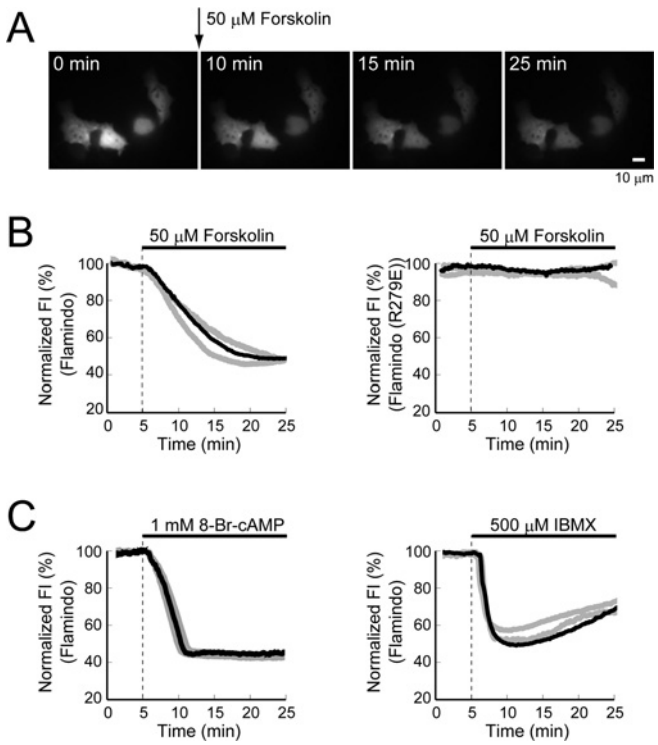

Figure 3 Epifluorescence imaging of Flamindo in COS7 cells

(**A**) Typical sequential images of Flamindo-expressing COS7 cells stimulated with 50 μM forskolin. (**B**) Time course of intracellular cAMP concentration ($[cAMP]_i$) changes in cells expressing either Flamindo (left-hand panel) or Flamindo (R279E) (right-hand panel) during 50 μM forskolin stimulation. (**C**) Time course of $[cAMP]_i$ changes in Flamindo-expressing COS7 cells during 1 mM 8-Br-cAMP (left-hand panel) or 500 μM IBMX (right-hand panel) stimulation. Three traces from independent experiments are shown in all graphs.

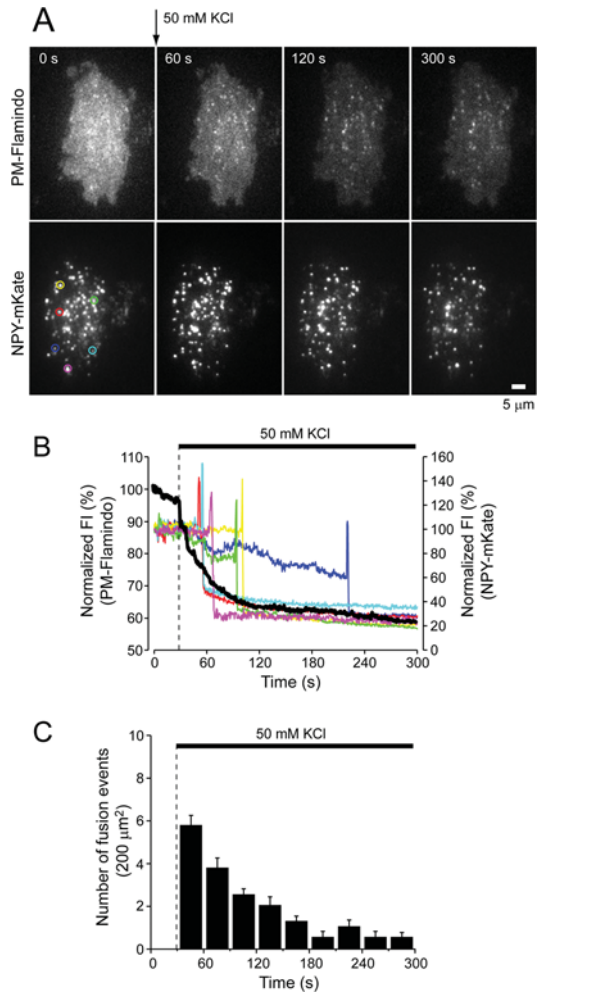

Figure 4 Simultaneous TIRF imaging of cAMP and exocytosis in the pancreatic β-cell line MIN6

(**A**) Typical sequential TIRF images of MIN6 cells expressing the plasma-membrane-targeted Flamindo (top panels) and NPY–mKate (bottom panels) stimulated with high-KCl (50 mM). (**B**) Time course of cAMP concentration at the plasma membrane (thick black trace) and exocytosis (coloured traces). Each colour corresponds to the fluorescence intensities of circles shown in (**A**). All traces were normalized to a start value of 100 %. (**C**) The number of fusion events was counted every 30 s. The results shown are the means $\pm$ S.E.M.

cAMP (1 mM) decreased the fluorescence intensity of Flamindo by half, suggesting that the cAMP-unbound form of Flamindo was 2-fold brighter than the cAMP-bound form. Consistently the absorption of Flamindo also decreased slightly at approximately 500 nm (Figure 2B). We next analysed the dissociation constant (K_d) values of Flamindo for both cAMP and cGMP by titration. Plots were fitted using a Hill equation (Figure 2C). A calculation of the K_d values by analysis of the titration curve of Flamindo yielded 3.6 μM and 29.9 μM for cAMP and cGMP respectively. Similar K_d values were reported previously for cAMP and cGMP [24,25]. Hill coefficients for cAMP and cGMP were 1.31 and 1.33 respectively. We also found that Flamindo displayed pH-dependent fluorescence intensity changes (Figure 2D) similar to that of other single wavelength indicators on the basis of circularly permutated fluorescent proteins (i.e. pericam and G-CaMP) or responsive-element-inserted fluorescent proteins (i.e. Camgaroo) [21,26,27]. The pH titration curves of Flamindo indicate that the mechanism of cAMP-dependent change in fluorescence intensity is associated with the protonation/deprotonation equilibrium of the chromophore.

cAMP imaging in COS7 cells expressing Flamindo with cAMP-evoking stimuli

We monitored the fluorescence intensity change in Flamindo-expressing COS7 cells during application of cAMP-producing reagents. Flamindo was distributed throughout both the cytosolic and nuclear compartments in COS7 cells as expected for a 45 kDa protein without a targeting signal sequence (Figure 3A). Application of 50 μM forskolin substantially decreased the fluorescence intensity within several seconds and reached a plateau after 20 min (Figure 3B, left-hand side). We next applied a phosphodiesterase inhibitor (IBMX) and a cAMP analogue (8-Br-cAMP) to the cells. Application of both IBMX and 8-Br-cAMP rapidly induced a decrease in Flamindo fluorescence intensity, whereas substantial recovery of the fluorescence intensity was only observed following IBMX stimulation (Figure 3C).

To verify that the decrease in fluorescence intensity in Flamindo-expressed COS7 cells was caused by $[cAMP]_i$ changes, we created mutant Flamindo [Flamindo (R279E)]. This mutation was shown to disrupt the cAMP-binding site of Epac1 [28]. Although the expression pattern of Flamindo (R279E) is indistinguishable from that of Flamindo in both COS7 and MIN6 cells (results not shown), no change in fluorescence intensity was observed in forskolin-treated cells (Figure 3B).

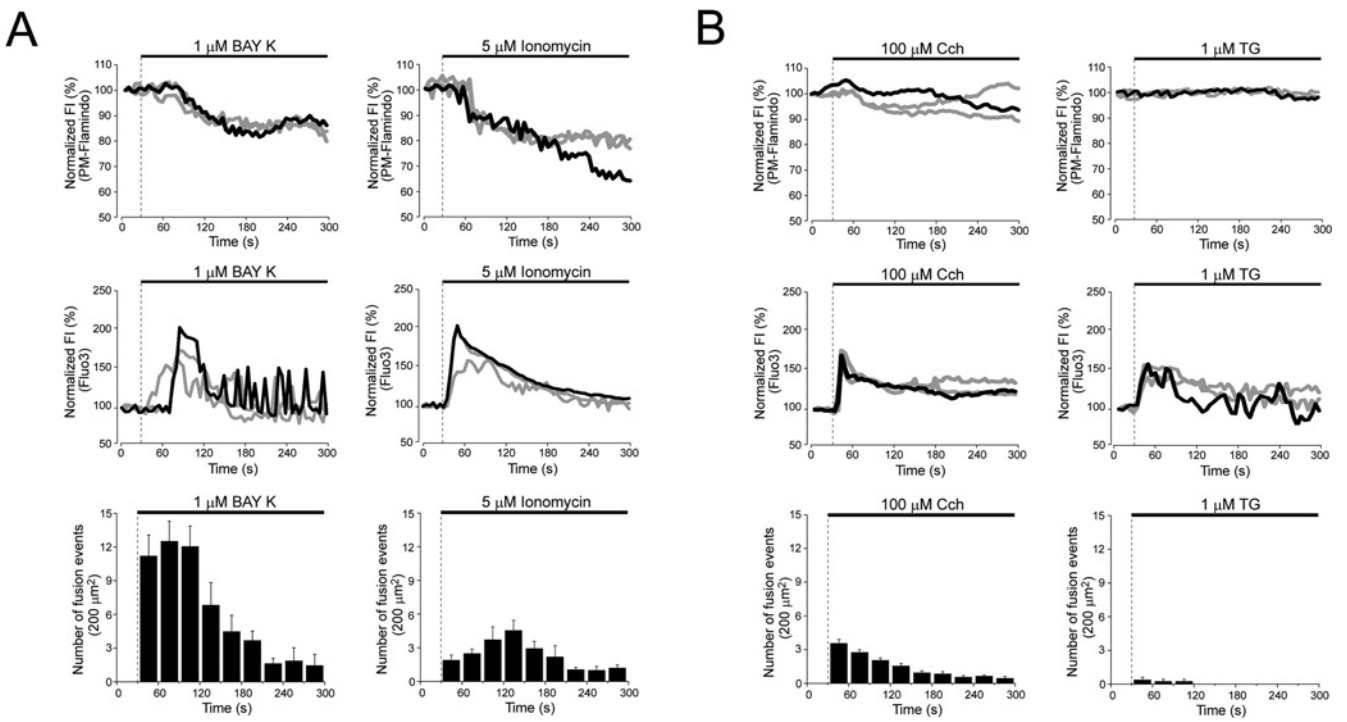

Figure 5 TIRF imaging of cAMP (PM-Flamindo), Ca^{2+} (Fluo3) and exocytosis (NPY–mKate) with Ca^{2+}-elevating reagents

(**A**) Time course of cAMP concentration changes at the plasma membrane ($[cAMP]_i$) (top panels), Ca^{2+} ($[Ca^{2+}]_i$) (middle panels) and exocytosis (bottom panels) with reagents that induce extracellular Ca^{2+} influx in MIN6 cells. (**B**) Time courses of $[cAMP]_i$ (top panels), $[Ca^{2+}]_i$ (middle panels) and exocytosis (bottom panels) with reagents that induce Ca^{2+} mobilization from internal stores in MIN6 cells. Three traces from independent experiments are shown in all graphs. All traces were normalized to a start value of 100 %. The number of fusion events was counted every 30 s. The results shown are the means ± S.E.M.

cAMP imaging in MIN6 cells expressing Flamindo

To monitor the dynamics of $[cAMP]_i$ beneath the plasma membrane and exocytosis simultaneously, we co-transfected PM-Flamindo (plasma-membrane-targeted Flamindo) and NPY–mKate into MIN6 cells. We visualized the two events using dual-colour TIRF microscopy (Figure 4A). We found that fusion of the GAP43 (neuromodulin) fragment to the N-terminus of Flamindo improved the signal-to-noise ratio of TIRF images (Figure 1, bottom panel). PM-Flamindo and NPY–mKate exhibited uniform distribution on the plasma membrane and punctate structures beneath the plasma membrane respectively (Figure 4A). Application of high-KCl caused an immediate decrease in fluorescence intensity of PM-Flamindo (Figure 4B, thick black trace), a transient increase in mKate fluorescence at multiple sites, which corresponded to exocytosis of NPY–mKate-containing vesicles (Figure 4B, coloured traces) and exocytosis (Figure 4C). These results indicate that Flamindo is suitable for the simultaneous imaging of two physiological events (i.e. cAMP and exocytosis, or cAMP and endocytosis) in same cells under a dual-colour TIRF microscope, whereas FRET-based indicators require the highly technical triple-colour TIRF microscope.

$[cAMP]_i$ is induced by an extracellular Ca^{2+} influx in MIN6 cells

Because high-KCl stimulation induced the increase of $[cAMP]_i$ in MIN6 cells (Figure 4), we wanted to identify what molecule(s) regulates $[cAMP]_i$ changes in these cells. We thus observed the dynamics of $[cAMP]_i$ and $[Ca^{2+}]_i$ beneath the plasma membrane and exocytosis after application of various Ca^{2+}-elevating reagents by TIRF microscopy. Induction of extracellular Ca^{2+} influx by application of the L-type Ca^{2+} channel agonist BAY K8664 and Ca^{2+} ionophore ionomycin provoked the increase of $[cAMP]_i$ and exocytosis (Figure 5A). By contrast, mobilization of intracellular Ca^{2+} by application of the muscarinic receptor agonist Cch or the endoplasmic reticulum Ca^{2+}-ATPase inhibitor TG had little effect on $[cAMP]_i$ (Figure 5B, top panels). It should be noted that exocytosis was induced by Cch, but not by TG (Figure 5B, bottom panel). These results suggest that an influx of extracellular Ca^{2+} is essential for $[cAMP]_i$ changes, and that the elevation of cAMP is not prerequisite for exocytosis in MIN6 cells.

We next monitored the dynamics of $[cAMP]_i$, $[Ca^{2+}]_i$ and exocytosis after application of various cAMP-elevating reagents. Although all cAMP-elevating reagents induced a few exocytotic events, $[Ca^{2+}]_i$ elevation was induced by forskolin and IBMX, whereas subtle $[Ca^{2+}]_i$ elevation was induced by 8-bromo-cAMP (Figure 6). These data indicated that endogenous cAMP production was required to induce $[Ca^{2+}]_i$ elevation.

ADCY1 is involved in extracellular Ca^{2+} entry-dependent cAMP production

The results described above so far indicate that extracellular Ca^{2+} influxes induce an increase in $[cAMP]_i$ beneath the plasma membrane. The mammalian ADCY consists of a large family of enzymes that convert ATP into cAMP; there are nine membrane-bound members (ADCY1–9) and one soluble member (ADCY10) [29,30]. Because ADCYs 1, 5, 6 and 8 are sensitive to Ca^{2+}, it is possible that the increase in $[cAMP]_i$ observed in MIN6 cells is due to the function of these ADCYs.

To identify which ADCYs are expressed in MIN6 cells, we performed RT–PCR analysis and found that *Adcy1*,

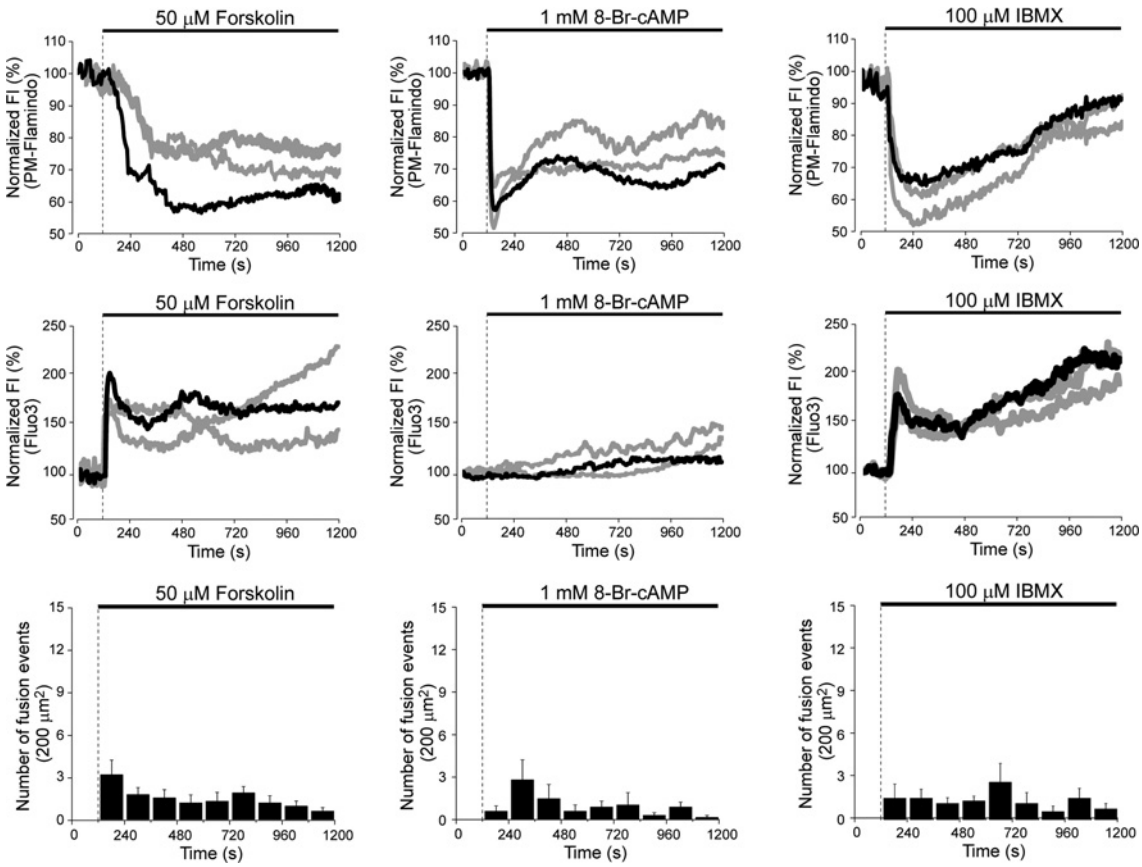

Figure 6 TIRF imaging of cAMP (PM-Flamindo), Ca^{2+} (Fluo3) and exocytosis (NPY–mKate) with cAMP-elevating reagents

Time course of $[cAMP]_i$ (top panels), $[Ca^{2+}]_i$ (middle panels) and exocytosis (bottom panels) in MIN6 cells. Three traces from independent experiments are shown in all graphs. All traces were normalized to a start value of 100 %. The number of fusion events was counted every 120 s. The results shown are the means ± S.E.M.

Adcy6, *Adcy7* and *Adcy9* were expressed in MIN6 cells (Figure 7). Because ADCY1 is the only enzyme activated by an extracellular Ca^{2+} influx within ADCY1, 6, 7 and 9, we speculated that ADCY1 is responsible for the high-KCl- and glucose-induced $[cAMP]_i$ changes. To examine the function of ADCY1, we depleted the endogenous *Adcy1* gene by the expression of specific siRNA against ADCY1. To verify the silencing efficiency of ADCY1 siRNA, we first checked the expression of ADCY1 mRNA and protein in the cells. We found that the ADCY1 siRNA significantly suppressed the expression of both ADCY1 mRNA and protein (Figures 8A and 8B). We also found that the silencing of endogenous ADCY1 by siRNA significantly suppressed both $[cAMP]_i$ and $[Ca^{2+}]_i$ changes after application of glucose (Figure 8C, top and middle panels of the right-hand column) without affecting the expression of L-type Ca^{2+} channels (Figure 8A). Furthermore, the number of fusion events were suppressed (Figure 8C, bottom panels of the right-hand column). Knockdown of endogenous ADCY1 by different siRNA targeting sequences for ADCY1 (see Supplementary Table S1) or the application of the ADCY inhibitor DDA to the cells showed significant suppression of both $[cAMP]_i$ and $[Ca^{2+}]_i$ changes after application of glucose (Supplementary Figure S2 at http://www.biochemj.org/bj/450/bj4500365add.htm). Taken together, these results indicate that ADCY1 is involved in extracellular Ca^{2+} influx-dependent cAMP production in the pancreatic β-cell line MIN6 cells.

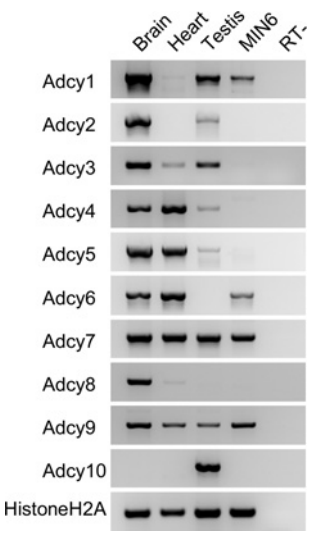

Figure 7 Expression profile of the *Adcy* family in MIN6 cells revealed by RT-PCR analysis

The ubiquitous marker histone H2A served as a control. PCR without reverse transcription was performed to verify genomic DNA and/or other contaminations (RT-).

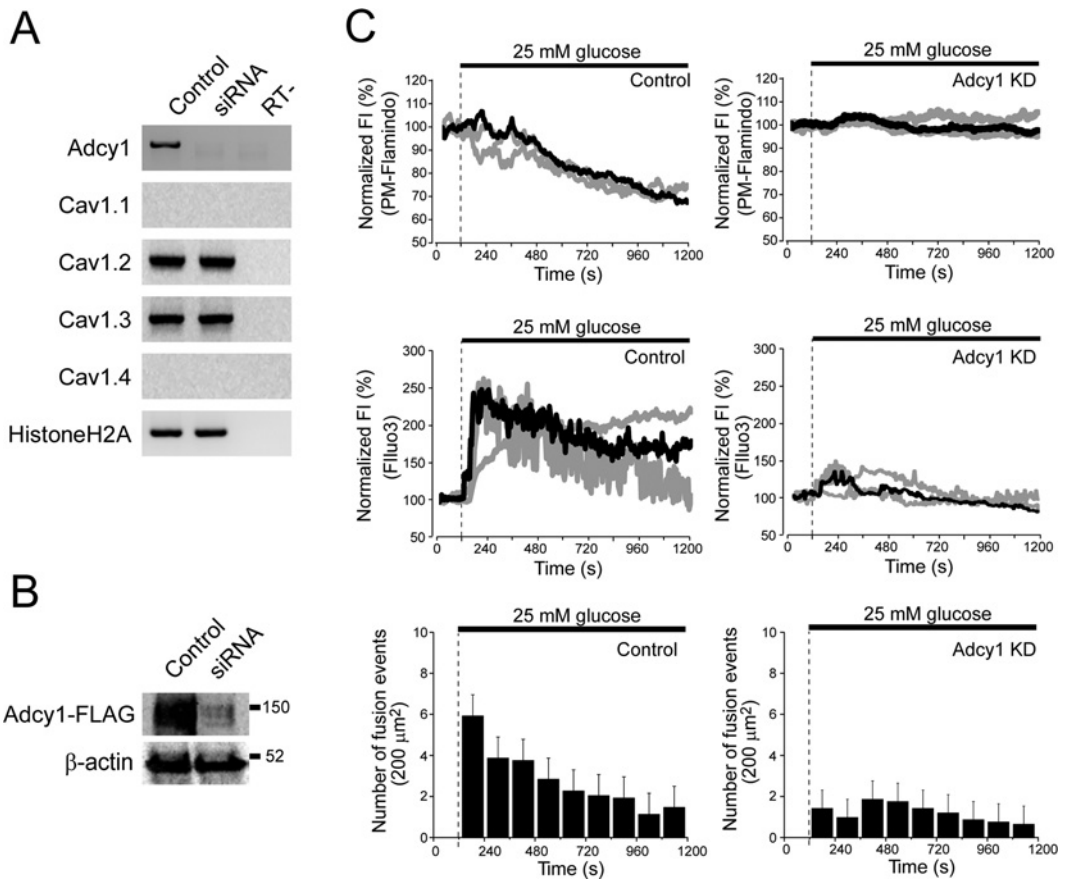

Figure 8 Effect of silence of ADCY1 on $[cAMP]_i$, $[Ca^{2+}]_i$ and exocytosis

(**A**) Expression of endogenous *Adcy1* and L-type Ca^{2+} channels in MIN6 cells with scramble RNA (control) or ADCY1-targeted siRNA (siRNA) revealed by RT–PCR. (**B**) Effect of ADCY1 siRNA on expression of ADCY1–FLAG in COS7 cells revealed by immunoblotting with an anti-FLAG or anti-β-actin antibody. The positions of the molecular mass markers (in kDa) are shown on the right. (**C**) Time course of $[cAMP]_i$ with glucose stimulation in Flamindo-expressing MIN6 cells (top panels) with scramble siRNA (Control) or ADCY1 siRNA (Adcy1 KD). Time course of $[Ca^{2+}]_i$ with glucose stimulation in Fluo3-loaded MIN6 cells with scramble siRNA or ADCY1 siRNA (middle panels). Three traces from independent experiments are shown in all graphs. All traces were normalized to a start value of 100 %. The number of fusion events was counted every 120 s (bottom panels). The results shown are the means ± S.E.M.

DISCUSSION

Of the ten members of ADCYs, four are Ca^{2+}-sensitive. ADCY1 and ADCY8 are activated by extracellular Ca^{2+} influx, and ADCY5 and ADCY6 are inhibited by extracellular Ca^{2+} influx in mammalian tissues [29,30]. It has been suggested that ADCY8 selectively responds to store-operated Ca^{2+} entry via the Ca^{2+} release-activated Ca^{2+} channel protein 1 Orai1 [31,32]. Although we could not detect the expression of *Adcy8* in our MIN6 cells (Figure 8A) [18], both *Adcy1* and *Adcy8* was observed in rat native pancreatic β-cells and cell lines [33]. This discrepancy could be attributed to the differences between species, cell lines or clones of the cell lines. Since *Adcy8* is expressed in native β-cells and ADCY8 plays a crucial role in store-operated Ca^{2+} entry [31,32], each member of the ADCY family would be regulated by extracellular Ca^{2+} influx through each distinct pathway in native β-cells for insulin secretion.

In the present study, we have shown that extracellular Ca^{2+} influx from L-type Ca^{2+} channels activates ADCY1, which exists on the plasma membrane. On the basis of these findings, we propose a new model for insulin secretion (Figure 9). Stimulation by both high-KCl and glucose depolarizes the membrane potential in the pancreatic β-cell line MIN6. Membrane depolarization opens VOCCs, and Ca^{2+} ions are mobilized from the extracellular space to the cytosol through VOCCs. The Ca^{2+} ions entering via VOCCs activate ADCY1, which is located close to VOCCs, and induce $[cAMP]_i$ changes. The increase in $[cAMP]_i$ further enhances the extracellular Ca^{2+} influx through modification of VOCCs and Ca^{2+}-activated non-selective cation channels for facilitating exocytosis [5]. This model was supported by the result that the silencing of endogenous ADCY1 by ADCY1 siRNA did not alter the expression of L-type calcium channels (Figure 8A).

Cch and TG induce Ca^{2+} mobilization from the internal Ca^{2+} store by opening IP_3 (inositol 1,4,5-trisphosphate) receptors and inhibiting the Ca^{2+} pump respectively. On the other hand, BAY K 8644 and ionomycin cause extracellular Ca^{2+} influx through L-type Ca^{2+} channels and Ca^{2+} permeation on the plasma membrane respectively. Although all of these agents induce $[Ca^{2+}]_i$ changes in MIN6 cells, $[cAMP]_i$ changes were only induced by extracellular Ca^{2+} influx but not induced by Ca^{2+} mobilization from internal Ca^{2+} stores (Figure 5). Because many ADCYs were located on the plasma membrane, the extracellular Ca^{2+} influx-dependent $[cAMP]_i$ changes may be explained by the distance between ADCY and the Ca^{2+} entry site at the plasma membrane. Namely, the high Ca^{2+} concentration at the Ca^{2+} entry site activates Ca^{2+}-sensitive ADCY, which is located in close vicinity to the entry site. We found that Cch induced exocytosis without the elevation of $[cAMP]_i$ changes (Figure 5B). In addition to Ca^{2+} mobilization from internal Ca^{2+} stores, Ach (acetylcholine) is involved in the complex signal

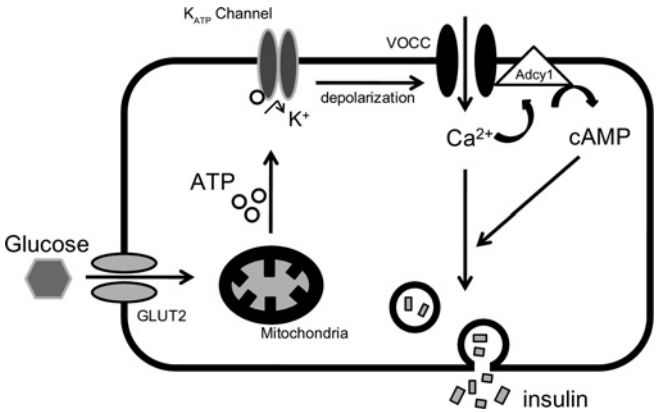

Figure 9 Proposed model of interplay between cAMP dynamics and extracellular Ca^{2+} influx

Ca^{2+} entry through VOCCs activates ADCY1 to facilitate vesicle fusion.

transduction mechanism of insulin secretion in pancreatic β-cells [34]. Thus exocytosis induced by Cch might be regulated by both Ca^{2+} mobilization and the complex signal transduction mechanism. The enhancement of cAMP production by forskolin and IBMX could occur in the vicinity of the Ca^{2+} entry site, whereas the membrane-permeant cAMP analogue 8-bromo-cAMP increased cAMP concentrations throughout the cell. As a result, forskolin and IBMX induced the increase in $[Ca^{2+}]_i$, but 8-bromo-cAMP did not. Therefore the local concentration of both Ca^{2+} and cAMP is necessary for their mutual interaction.

In the present study, we also measured the absorption spectrum of Flamindo at pH 7.4 (Figure 2B). Flamindo displayed a major absorption wavelength maximum at 418 nm with a slight shoulder at approximately 500 nm, in contrast with the major absorption peak at 514 nm in Citrine. This blue shift was consistent with the absorption spectrum of circular permutated EYFP (enhanced YFP) [26,35], suggesting that the chromophore was protonated in Flamindo. As shown in Figure 2(A), the peak of excitation/emission in Flamindo (506/521 nm) was similar to that of Citrine (514/524 nm). Because the peak excitation was 506 nm, a small absorption at approximately 500 nm in Flamindo is thought to contribute to excitation. Flamindo showed a weaker fluorescence intensity than Citrine in both mammalian and bacterial cells because of the small absorption at approximately 500 nm. To create a brighter mutant of Flamindo, we replaced Citrine with other GFP (green fluorescent protein) variants (i.e. Venus and superfolder GFP) to improve brightness by enhancing its folding [36,37]. Although both of the new mutants showed brighter fluorescence in mammalian cells, the sensitivity to cAMP was completely abolished (results not shown), suggesting that enhancing the folding of Flamindo resulted in a lack of fluorescence intensity change following the cAMP-binding-induced conformational change. Therefore we concluded that there is a trade-off between the fluorescence intensity and cAMP sensitivity in Flamindo.

Previous studies have demonstrated that Ca^{2+} microdomains were implicated in regulating the kinetics of dense-core vesicle exocytosis [9]. Additionally, in cardiac myocytes, β-adrenergic stimulation generated multiple microdomains with $[cAMP]_i$ changes [38]. In the present study, we showed a spatial and temporal relationship between exocytosis and $[cAMP]_i$ changes in the pancreatic β-cell line MIN6. Although the fluorescence intensity of Flamindo was decreased by stimulation (Figure 4A), no obvious cAMP microdomains in MIN6 cells were observed under the TIRF microscope. Expansion of the dynamic range of Flamindo and/or a variant of Flamindo, or increasing fluorescence intensity by $[cAMP]_i$ changes, would enable us to detect the microdomains of cAMP in mammalian cells. Further improvements to Flamindo are needed to observe the spatial dynamics of $[cAMP]_i$ at a better resolution.

In summary, we have developed a single fluorescent protein-based cAMP indicator, Flamindo, and found that Ca^{2+}-sensitive ADCY is implicated in glucose-induced $[cAMP]_i$ changes in the pancreatic β-cell line MIN6. Because $[cAMP]_i$ changes by glucagon-like peptide-1 and gastric inhibitory polypeptide were only identified in the cAMP-elevating signalling pathway, this new Ca^{2+}-sensitive ADCY-dependent Ca^{2+} influx-induced cAMP-producing pathway may be a new drug target for diabetes mellitus.

AUTHOR CONTRIBUTION

Tetsuya Kitaguchi, Manami Oya, Yoshiko Wada and Takashi Tsuboi conceived the experiments. Tetsuya Kitaguchi, Takashi Tsuboi and Atsushi Miyawaki co-wrote the paper. Atsushi Miyawaki provided scientific guidance and financial support. All authors discussed the results and commented on the paper.

ACKNOWLEDGEMENTS

We thank Professor Susumu Seino for the gift of MIN6 cells. We are grateful to members of the Miyawaki Laboratory at RIKEN Brain Science Institute and ERATO Japan Science and Technology Agency for valuable discussions.

FUNDING

This work was supported, in part, by the Ministry of Education, Culture, Sports, Science and Technology of Japan [grant numbers 22790197 (to T.K.), 24790207 (to T.T.)], the JGC-S Scholarship Foundation (to T.K.), the Nestlé Nutrition Council, Japan (to T.T.), the Mishima Kaiun Memorial Foundation (to T.T.) and the Takeda Science Foundation (to T.T.).

REFERENCES

1 Henquin, J. C. (2000) Triggering and amplifying pathways of regulation of insulin secretion by glucose. Diabetes **49**, 1751–1760
2 Rorsman, P., Eliasson, L., Renstrom, E., Gromada, J., Barg, S. and Gopel, S. (2000) The cell physiology of biphasic insulin secretion. News Physiol. Sci. **15**, 72–77
3 Gembal, M., Gilon, P. and Henquin, J. C. (1992) Evidence that glucose can control insulin release independently from its action on ATP-sensitive K^+ channels in mouse B cells. J. Clin. Invest. **89**, 1288–1295
4 Borodinsky, L. N. and Spitzer, N. C. (2006) Second messenger pas de deux: the coordinated dance between calcium and cAMP. Sci. STKE **2006**, pe22
5 Seino, S. and Shibasaki, T. (2005) PKA-dependent and PKA-independent pathways for cAMP-regulated exocytosis. Physiol. Rev. **85**, 1303–1342
6 Landa, Jr, L. R., Harbeck, M., Kaihara, K., Chepurny, O., Kitiphongspattana, K., Graf, O., Nikolaev, V. O., Lohse, M. J., Holz, G. G. and Roe, M. W. (2005) Interplay of Ca^{2+} and cAMP signaling in the insulin-secreting MIN6 β-cell line. J. Biol. Chem. **280**, 31294–31302
7 Tsuboi, T., McMahon, H. T. and Rutter, G. A. (2004) Mechanisms of dense core vesicle recapture following "kiss and run" ("cavicapture") exocytosis in insulin-secreting cells. J. Biol. Chem. **279**, 47115–47124
8 Ohara-Imaizumi, M., Fujiwara, T., Nakamichi, Y., Okamura, T., Akimoto, Y., Kawai, J., Matsushima, S., Kawakami, H., Watanabe, T., Akagawa, K. and Nagamatsu, S. (2007) Imaging analysis reveals mechanistic differences between first- and second-phase insulin exocytosis. J. Cell Biol. **177**, 695–705
9 Becherer, U., Moser, T., Stuhmer, W. and Oheim, M. (2003) Calcium regulates exocytosis at the level of single vesicles. Nat. Neurosci. **6**, 846–853
10 Zaccolo, M., De Giorgi, F., Cho, C. Y., Feng, L., Knapp, T., Negulescu, P. A., Taylor, S. S., Tsien, R. Y. and Pozzan, T. (2000) A genetically encoded, fluorescent indicator for cyclic AMP in living cells. Nat. Cell Biol. **2**, 25–29
11 Nikolaev, V. O., Bunemann, M., Hein, L., Hannawacker, A. and Lohse, M. J. (2004) Novel single chain cAMP sensors for receptor-induced signal propagation. J. Biol. Chem. **279**, 37215–37218

12 Ponsioen, B., Zhao, J., Riedl, J., Zwartkruis, F., van der Krogt, G., Zaccolo, M., Moolenaar, W. H., Bos, J. L. and Jalink, K. (2004) Detecting cAMP-induced Epac activation by fluorescence resonance energy transfer: Epac as a novel cAMP indicator. EMBO Rep. **5**, 1176–1180

13 DiPilato, L. M., Cheng, X. and Zhang, J. (2004) Fluorescent indicators of cAMP and Epac activation reveal differential dynamics of cAMP signaling within discrete subcellular compartments. Proc. Natl. Acad. Sci. U.S.A. **101**, 16513–16518

14 Heikal, A. A., Hess, S. T., Baird, G. S., Tsien, R. Y. and Webb, W. W. (2000) Molecular spectroscopy and dynamics of intrinsically fluorescent proteins: coral red (dsRed) and yellow (Citrine). Proc. Natl. Acad. Sci. U.S.A. **97**, 11996–12001

15 de Rooij, J., Zwartkruis, F. J., Verheijen, M. H., Cool, R. H., Nijman, S. M., Wittinghofer, A. and Bos, J. L. (1998) Epac is a Rap1 guanine-nucleotide-exchange factor directly activated by cyclic AMP. Nature **396**, 474–477

16 Shcherbo, D., Merzlyak, E. M., Chepurnykh, T. V., Fradkov, A. F., Ermakova, G. V., Solovieva, E. A., Lukyanov, K. A., Bogdanova, E. A., Zaraisky, A. G., Lukyanov, S. and Chudakov, D. M. (2007) Bright far-red fluorescent protein for whole-body imaging. Nat. Methods **4**, 741–746

17 Mizushima, S. and Nagata, S. (1990) pEF-BOS, a powerful mammalian expression vector. Nucleic Acids Res. **18**, 5322

18 Minami, K., Yano, H., Miki, T., Nagashima, K., Wang, C. Z., Tanaka, H., Miyazaki, J. I. and Seino, S. (2000) Insulin secretion and differential gene expression in glucose-responsive and -unresponsive MIN6 sublines. Am. J. Physiol. Endocrinol. Metab. **279**, E773–E781

19 Tsuboi, T., Zhao, C., Terakawa, S. and Rutter, G. A. (2000) Simultaneous evanescent wave imaging of insulin vesicle membrane and cargo during a single exocytotic event. Curr. Biol. **10**, 1307–1310

20 Mamo, S., Gal, A. B., Bodo, S. and Dinnyes, A. (2007) Quantitative evaluation and selection of reference genes in mouse oocytes and embryos cultured *in vivo* and *in vitro*. BMC Dev. Biol. **7**, 14

21 Baird, G. S., Zacharias, D. A. and Tsien, R. Y. (1999) Circular permutation and receptor insertion within green fluorescent proteins. Proc. Natl. Acad. Sci. U.S.A. **96**, 11241–11246

22 Griesbeck, O., Baird, G. S., Campbell, R. E., Zacharias, D. A. and Tsien, R. Y. (2001) Reducing the environmental sensitivity of yellow fluorescent protein. Mechanism and applications. J. Biol. Chem. **276**, 29188–29194

23 Rehmann, H., Prakash, B., Wolf, E., Rueppel, A., de Rooij, J., Bos, J. L. and Wittinghofer, A. (2003) Structure and regulation of the cAMP-binding domains of Epac2. Nat. Struct. Biol. **10**, 26–32

24 de Rooij, J., Rehmann, H., van Triest, M., Cool, R. H., Wittinghofer, A. and Bos, J. L. (2000) Mechanism of regulation of the Epac family of cAMP-dependent RapGEFs. J. Biol. Chem. **275**, 20829–20836

25 Dao, K. K., Teigen, K., Kopperud, R., Hodneland, E., Schwede, F., Christensen, A. E., Martinez, A. and Doskeland, S. O. (2006) Epac1 and cAMP-dependent protein kinase holoenzyme have similar cAMP affinity, but their cAMP domains have distinct structural features and cyclic nucleotide recognition. J. Biol. Chem. **281**, 21500–21511

26 Nagai, T., Sawano, A., Park, E. S. and Miyawaki, A. (2001) Circularly permuted green fluorescent proteins engineered to sense Ca^{2+}. Proc. Natl. Acad. Sci. U.S.A. **98**, 3197–3202

27 Nakai, J., Ohkura, M. and Imoto, K. (2001) A high signal-to-noise Ca^{2+} probe composed of a single green fluorescent protein. Nat. Biotechnol. **19**, 137–141

28 Steinberg, R. A., Symcox, M. M., Sollid, S. and Ogreid, D. (1996) Arginine 210 is not a critical residue for the allosteric interactions mediated by binding of cyclic AMP to site A of regulatory (RIα) subunit of cyclic AMP-dependent protein kinase. J. Biol. Chem. **271**, 27630–27636

29 Defer, N., Best-Belpomme, M. and Hanoune, J. (2000) Tissue specificity and physiological relevance of various isoforms of adenylyl cyclase. Am. J. Physiol. Renal Physiol. **279**, F400–F416

30 Hanoune, J. and Defer, N. (2001) Regulation and role of adenylyl cyclase isoforms. Annu. Rev. Pharmacol. Toxicol. **41**, 145–174

31 Martin, A. C., Willoughby, D., Ciruela, A., Ayling, L. J., Pagano, M., Wachten, S., Tengholm, A. and Cooper, D. M. (2009) Capacitative Ca^{2+} entry via Orai1 and stromal interacting molecule 1 (STIM1) regulates adenylyl cyclase type 8. Mol. Pharmacol. **75**, 830–842

32 Masada, N., Ciruela, A., Macdougall, D. A. and Cooper, D. M. (2009) Distinct mechanisms of regulation by Ca^{2+}/calmodulin of type 1 and 8 adenylyl cyclases support their different physiological roles. J. Biol. Chem. **284**, 4451–4463

33 Delmeire, D., Flamez, D., Hinke, S. A., Cali, J. J., Pipeleers, D. and Schuit, F. (2003) Type VIII adenylyl cyclase in rat beta cells: coincidence signal detector/generator for glucose and GLP-1. Diabetologia **46**, 1383–1393

34 Gilon, P. and Henquin, J. C. (2001) Mechanisms and physiological significance of the cholinergic control of pancreatic β-cell function. Endocr. Rev. **22**, 565–604

35 Topell, S., Hennecke, J. and Glockshuber, R. (1999) Circularly permuted variants of the green fluorescent protein. FEBS Lett. **457**, 283–289

36 Nagai, T., Ibata, K., Park, E. S., Kubota, M., Mikoshiba, K. and Miyawaki, A. (2002) A variant of yellow fluorescent protein with fast and efficient maturation for cell-biological applications. Nat. Biotechnol. **20**, 87–90

37 Pedelacq, J. D., Cabantous, S., Tran, T., Terwilliger, T. C. and Waldo, G. S. (2006) Engineering and characterization of a superfolder green fluorescent protein. Nat. Biotechnol. **24**, 79–88

38 Zaccolo, M. and Pozzan, T. (2002) Discrete microdomains with high concentration of cAMP in stimulated rat neonatal cardiac myocytes. Science **295**, 1711–1715

Received 22 June 2012/4 December 2012; accepted 3 January 2013
Published as BJ Immediate Publication 3 January 2013, doi:10.1042/BJ20121022

Biochem. J. (2013) **450**, 365–373 (Printed in Great Britain) doi:10.1042/BJ20121022

SUPPLEMENTARY ONLINE DATA

Extracellular calcium influx activates adenylate cyclase 1 and potentiates insulin secretion in MIN6 cells

Tetsuya KITAGUCHI*†‡[1], Manami OYA§, Yoshiko WADA*†, Takashi TSUBOI§ and Atsushi MIYAWAKI*†[1]

*Life Function and Dynamics, ERATO, JST (Japan Science and Technology Agency), 2-1 Hirosawa, Wako, Saitama 351-0198, Japan, †Laboratory for Cell Function and Dynamics, Advanced Technology Development Group, Brain Science Institute, RIKEN, 2-1 Hirosawa, Wako, Saitama 351-0198, Japan, ‡Cell Signaling Group, Waseda Bioscience Research Institute in Singapore (WABOIS), Waseda University, 11 Biopolis Way, #05-01/02 Helios, Singapore 138667, Singapore, and §Department of Life Sciences, Graduate School of Arts and Sciences, The University of Tokyo, 3-8-1 Komaba, Meguro, Tokyo 153-8902, Japan

Table S1 Sequences of siRNA used in knockdown experiment

siRNA name	siRNA sense (5′→3′)	siRNA antisense (5′→3′)
ADCY1 siRNA	GCUUAUCUACCUUCUGGUAtt	UACCAGAAGGUAGAUAAGCtt
ADCY1 siRNA suppl	GUUCAAGACUGUGUGCUAUtt	AUAGCACACAGUCUUGAACtt

Table S2 DNA sequences of primers used for RT–PCR

Gene	Forward primer (5′→3′)	Reverse primer (5′→3′)
Adcy1	CGGATATCAAACCAGCCAAG	GACCACTAGGGAACTGTTAG
Adcy2	AGCATGACCACAGAGAATGG	TTGTCTCCTCAGAGTTGCTC
Adcy3	TTGTGGACATGCTCAGCTGT	AAGCGCTTGTGGTCGTATTC
Adcy4	GCCTTTATCAAAGCCCTTCG	ATGACTGCAGCTTCTCTCAG
Adcy5	CAAGAATGCCCAGGAAAGTG	GCGTTGTCGAAGAGTGTGAC
Adcy6	TCACGGAAAGTAGATCCTCG	GCCCATCAAAGGTCTCATTG
Adcy7	GCTACTGAGTTCTCGAGGTG	CAGCCGTGTCCTTTGTGTC
Adcy8	TTCCTACACCTTGACTGTGC	AGCCTGGGTATGAGTACTTG
Adcy9	ATGAGAGACCAGGCTGACTG	TCCGTGCACTTTGGGTAAAG
Adcy10	TCGAGTTAAGATAGGGCTGG	ATGGCTGAGCCTATGACTTC
Cav1.1	CCCCACTCAGATAGAGCTG	GATGTGGTTCATCTGTTCCG
Cav1.2	TACCGTCAGTTCCACACAG	CTTTCCCTCCTAGAGCATT
Cav1.3	ACCATGAGCACCTCTGCAC	GGTTCCCGCCTTCTGTTTC
Cav1.4	ACACTGAACCATACCGAGTG	GGTCATGAAGGTCTAACTCC
Histone *H2AFZ*	ACAGCGCAGCCATCCTGGAGTA	TTCCCGATCAGCGATTTGTGGA

[1] Correspondence may be addressed to either of these authors (email kitaguct@aoni.waseda.jp or matsushi@brain.riken.jp).

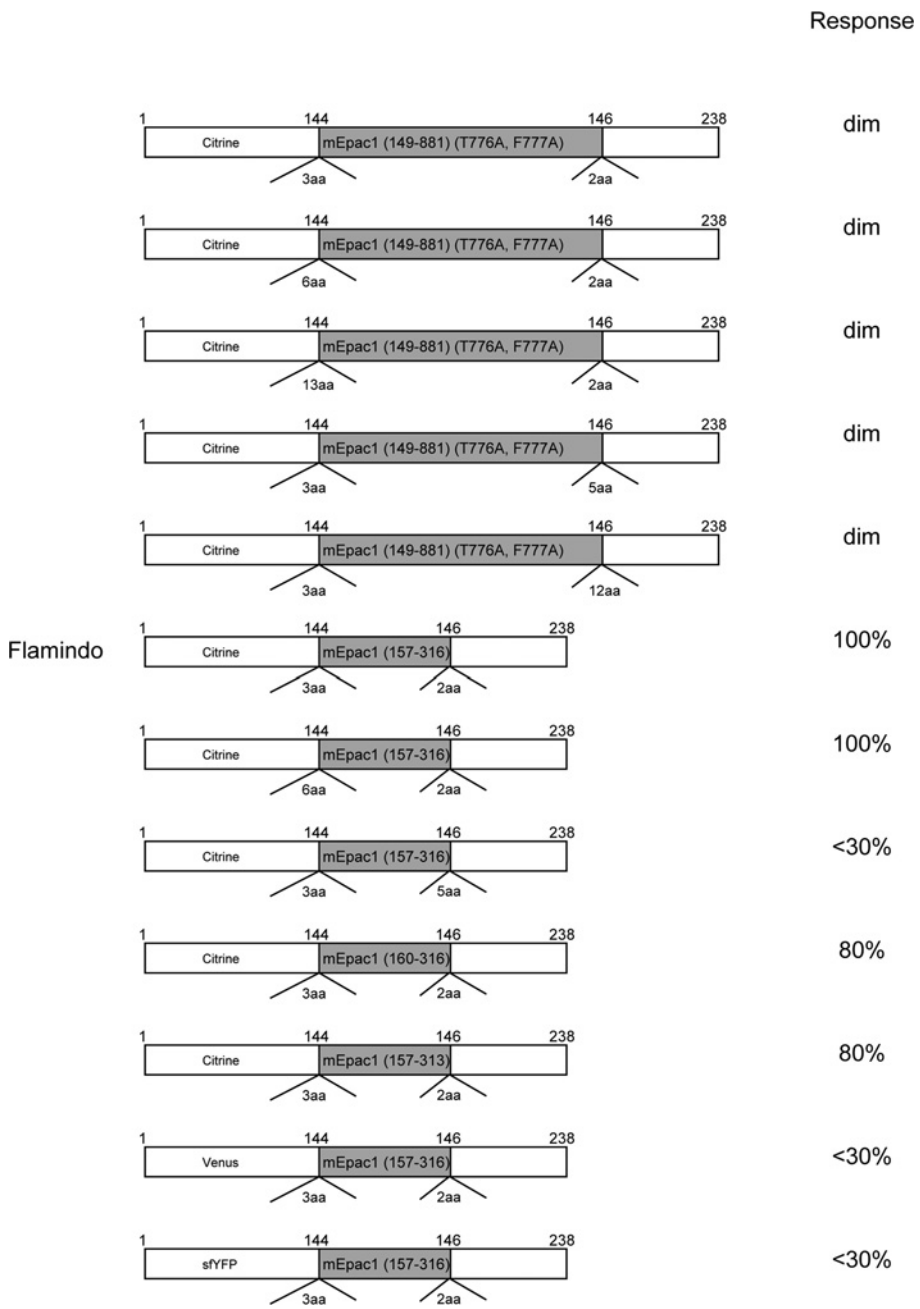

Figure S1 Schematic drawing of the structure of candidates for cAMP-responsive YFP

Cell lysates from fusion-protein-expressing JM109 (DE3) cells were subjected to fluorescence spectrophotometry with or without 1 mM cAMP. 'Response' indicates the relative change in fluorescence intensity against Flamindo following the addition of cAMP.

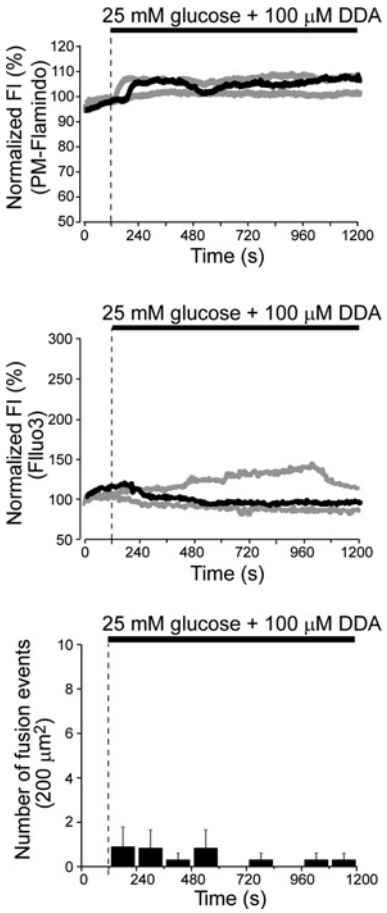

Figure S2 Effect of the ADCY inhibitor on $[cAMP]_i$, $[Ca^{2+}]_i$ and exocytosis

Time course of $[cAMP]_i$ with glucose stimulation in Flamindo-expressing MIN6 cells (top panels) with 100 μM DDA. Time course of $[Ca^{2+}]_i$ with glucose stimulation in Fluo3-loaded MIN6 cells with DDA (middle panel). Three traces from independent experiments are shown in all graphs. All traces were normalized to a start value of 100 %. The number of fusion events was counted every 120 s (bottom panels). The results shown are the means $\pm$ S.E.M.

Received 22 June 2012/4 December 2012; accepted 3 January 2013
Published as BJ Immediate Publication 3 January 2013, doi:10.1042/BJ20121022